



Cite this: *Nanoscale Adv.*, 2021, **3**, 2316

Carbon dots *versus* nano-carbon/organic hybrids – dramatically different behaviors in fluorescence sensing of metal cations with structural and mechanistic implications

Ping Wang,^a Mohammed J. Meziani,^{*b} Yingqiang Fu,^a Christopher E. Bunker,^{*c} Xiaofang Hou,^a Liju Yang,^{ID *d} Hind Msellek,^b Melina Zaharias,^a Jasmine P. Darby^d and Ya-Ping Sun^{ID *a}

Carbon dots (CDots) are defined as surface-passivated small carbon nanoparticles, with the effective passivation generally achieved by organic functionalization. Photoexcited CDots are both potent electron donors and acceptors, and their characteristic bright and colorful fluorescence emissions make them excellent fluorescence sensors for organic analytes and metal ions. For the latter extraordinarily low detection limits based on extremely efficient quenching of fluorescence intensities by the targeted metal cations have been observed and reported in the literature. However, all of the dot samples in those reported studies were made from "one-pot" carbonization of organic precursors mostly under rather mild processing conditions, unlikely to be sufficient for the required level of carbonization. Those dot samples should therefore be more appropriately considered as "nano-carbon/organic hybrids", characterized structurally as being highly porous and spongy, which must be playing a dominating role in the reported sensing results. In this study, we compared the dot samples from carbonization syntheses under similarly mild and also more aggressive processing conditions with the classically defined and structured CDots for the fluorescence sensing of copper(II) cations in aqueous solutions. The observed dramatic decoupling between quenching results for fluorescence intensities and lifetimes of the carbonization samples, with the former being extraordinary and the latter within the diffusion controlled limit, suggested that the quenching of fluorescence intensities was greatly affected by the higher local quencher concentrations than the bulk associated with the porous and spongy sample structures, especially for the sample from carbonization under too mild processing conditions. The major differences between the classical CDots and the nano-carbon/organic hybrids are highlighted, and the tradeoffs between sensitivity and accuracy or reproducibility in the use of the latter for fluorescence sensing are discussed.

Received 3rd January 2021
Accepted 24th February 2021

DOI: 10.1039/d1na00002k
rsc.li/nanoscale-advances

Introduction

Carbon "quantum" dots or carbon dots (CDots)^{1–3} have attracted much recent attention, with a wide variety of their potential technological applications explored,^{3–17} including especially those that would take advantage of their commonly observed

bright and colorful fluorescence emissions. In the relevant research community, the vivid display of the emissive properties has been used implicitly or explicitly as a characteristic signature for the formation or presence of CDots, even though there could be dramatic differences among samples from different syntheses in terms of composition, structure, and configuration.³

As originally reported and defined,^{1,3} CDots are surface-passivated small pre-existing carbon nanoparticles (Fig. 1), which represent the nanoscale carbon allotrope at zero-dimension.^{18,19} The surface passivation could be as minor as simple solvation in a solvent dispersion of the nanoparticles^{20–22} or some interactions with the matrix polymers when the nanoparticles are dispersed in polymeric films.²³ In both cases the passivation effect is generally weak, resulting in only minor improvements in the photoexcited state properties from those

^aDepartment of Chemistry and Laboratory for Emerging Materials and Technology, Clemson University, Clemson, South Carolina 29634, USA. E-mail: syaping@clemson.edu

^bDepartment of Natural Sciences, Northwest Missouri State University, Maryville, Missouri 64468, USA. E-mail: meziani@nwmissouri.edu

^cAir Force Research Laboratory, Propulsion Directorate, Wright-Patterson Air Force Base, Ohio 45433, USA. E-mail: christopher.bunker@wpafb.af.mil

^dDepartment of Pharmaceutical Sciences, Biomanufacturing Research Institute and Technology Enterprise, North Carolina Central University, Durham, NC 27707, USA. E-mail: lyang@nccu.edu



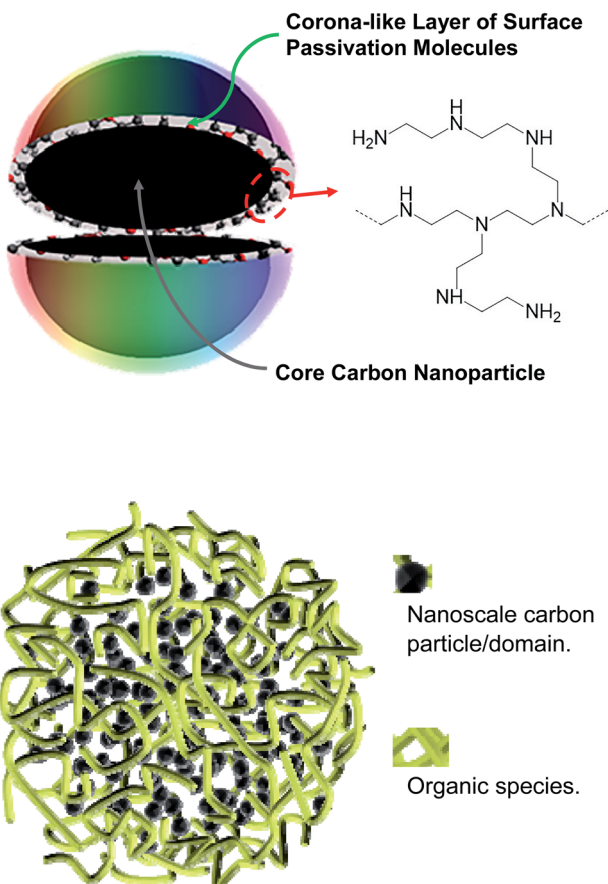


Fig. 1 Cartoons on (upper) CDots with oligomeric polyethylenimine for surface functionalization and (lower) dot-like structures in samples from carbonization syntheses in general (dubbed "nano-carbon/organic hybrids"), with the content and sizes of the nanoscale carbon domains dependent on the carbonization conditions.

of the largely “naked” carbon nanoparticles, as reflected by the observed slight increases in the brightness of fluorescence emissions.^{22,23} Considerably more effective passivation has been achieved *via* chemically functionalizing the surface of the small carbon nanoparticles with organic molecules or species (Fig. 1) for the truly bright and colorful fluorescence emissions,²⁴ among other distinctive photoexcited state properties and processes. These functionalized pre-existing carbon nanoparticles are the classically defined CDots.^{1,3}

As reported in the literature, however, majority of the dot samples used in fluorescence sensing and related studies have been prepared by thermally carbonizing various organic precursors under different yet generally rather mild processing conditions.^{8,13,25} Among more popular have been thermal or hydrothermal treatments of selected organic precursors mostly at a temperature around 200 °C, as low as 120 °C and rarely higher than 250 °C, for typically an hour or a few hours.⁸ Such samples have been used extensively as fluorescence quenching-based sensors for the detection and quantification of a wide variety of metal cations, including those of heavy metals and others such as copper. A common observation or outcome in such sensing of metal cations has been the ultrahigh sensitivity

for ultralow detection limits that are associated with the extraordinarily efficient quenching of fluorescence intensities by the metal cations for dot samples from carbonization syntheses. For example, the sample obtained by thermal carbonization of a citric acid–polyethylenimine mixture at 200 °C was used in the sensing of Cu^{2+} by fluorescence quenching to reach the detection limit down to $6 \times 10^{-9} \text{ M}$.²⁶ Similarly prepared samples were reported for the detection of 10^{-9} M of Cu^{2+} in aqueous solution,^{27–31} and also for the highly efficient fluorescence quenching by other metal cations,^{8,13} with the apparent slopes of the quenching plots (Φ_F^0/Φ_F versus cation concentration, where Φ_F^0 and Φ_F are fluorescence intensities without and with the quencher, respectively) as large as 530 000 M^{-1} .³²

Recently there have been major concerns and related debates on the compositions and structures of the samples obtained from carbonization syntheses,^{2,33–36} especially those with the use of processing conditions that are considered as being too mild for the carbonization to yield a significant amount of nanoscale carbon,³⁶ which should obviously be the critical ingredient in any *carbon* quantum dots. Even for those samples synthesized with more aggressive carbonization conditions, their nanoscale structures are largely unknown. One may argue that with the mostly random and chaotic conditions in the thermal or hydrothermal carbonization, there are no reasons to expect any thermodynamic or kinetic driving forces for the creation or formation of the well ordered nanostructure in the classically defined CDots (Fig. 1). More probably or likely would be the kind of structures, as also illustrated in Fig. 1, which are randomly crosslinked mixtures of organic species with various amounts of nanoscale carbon particles/domains for the cross-linking, depending on the processing conditions in the sample preparation and the resulting levels of carbonization. Such sample structures, expected logically to be rather porous, should have major effects on the quenching of their fluorescence emission intensities by metal cations, which are likely responsible for the often observed extraordinarily large quenching constants and the corresponding ultrahigh sensitivity in the fluorescence sensing. Such an assessment was evaluated and validated in the study reported here.

In the study, three different samples, including the classically defined CDots from the surface functionalization of pre-existing small carbon nanoparticles with oligomeric polyethylenimine (PEI) and the two dot samples obtained from the carbonization of citric acid-PEI mixtures under processing conditions of 200 °C for 3 h and 330 °C for 6 h, were compared for their fluorescence quenching-based sensing of copper cation (Cu^{2+}) in aqueous solutions. The dramatically different quenching results among the three samples, including the comparisons between quenchings of fluorescence intensities and lifetimes, suggest that major near-neighbor static quenching contributions must be responsible for the observed ultra-high sensitivity in the sensing based on the quenching of fluorescence intensities of the dot samples from carbonization syntheses. The implications of the results to the structures of the dot samples are rationalized and discussed.

Results and discussion

Mixtures of citric acid and oligomeric polyethylenimine (PEI) were used as precursors in the thermal carbonization processing under different experimental conditions.^{37,38} The samples from the processing in the presence of water in a sealed reactor at 200 °C and 330 °C are denoted as CS200 and CS330, respectively. Both samples in aqueous solutions are colored, though relatively the CS330 sample is significantly darker, indicative of a higher content of nanoscale carbon due to the more aggressive conditions in the carbonization processing.³⁸ Optical absorption spectra of the samples in aqueous solutions are shown in Fig. 2, which are in good agreement with those of the samples prepared from the same precursor mixtures under largely the same processing conditions.^{37,38} The spectrum of CS330 is red-shifted from that of CS200, consistent with the former in solution appearing relatively darker in color.

In a separate approach, selected pre-existing small carbon nanoparticles (~5 nm in average diameter) were functionalized with oligomeric polyethylenimine (PEI) in the microwave-assisted thermal reaction to obtain PEI-CDots.³⁹ Mechanistically the functionalization reaction was probably the nanoparticle surface addition of PEI-derived radical species created under the microwave radiation conditions.⁴⁰ The optical absorption spectrum of PEI-CDots in aqueous solution, also shown in Fig. 2, is close to that of the aqueous suspended small carbon nanoparticles used in the PEI functionalization, confirming that optical absorptions of the CDots are due to those of the core carbon nanoparticles (Fig. 1), as the organic

functionalization moieties (PEI species in PEI-CDots) are optically transparent in the corresponding spectral region. On the comparison of the three samples, the absorption spectrum of CS200 is clearly different, with significantly weaker absorptions in the visible (Fig. 2). However, as also compared in Fig. 2, the observed fluorescence spectra of the three samples at the same excitation wavelength (400 nm) are not so different.

The photoexcited states and fluorescence emissions of CDots are known for being susceptible to generally efficient quenching by both electron donor and acceptor molecules or species,⁴¹ including many metal cations as electron deficient quenchers.^{8,13,25} However, in studies reported in the literature on sensing various metal cations based on the quenching of fluorescence intensities with steady-state fluorescence emission measurements, overwhelming majority of the dot samples have been those similar to CS200, prepared by the carbonization of organic precursors under mild processing conditions. The corresponding linear quenching plots yielded extraordinarily large slopes as quenching constants, seemingly suggesting quenching processes much beyond the upper limit of diffusion control in aqueous or other liquid media, despite the fact the diffusion control must be absolute in all those media. Thus, most or all of those reported extreme quenching behaviors would have to be due to some specific or special characteristics of the used dot samples that could facilitate the similar extremes in terms of high “local quencher concentrations”, namely actual concentrations of the quencher in the immediate vicinity of the emissive entities being quenched are considerably higher than those in the bulk.^{42,43} Such local concentration or “static quenching” effects are made evident by results from

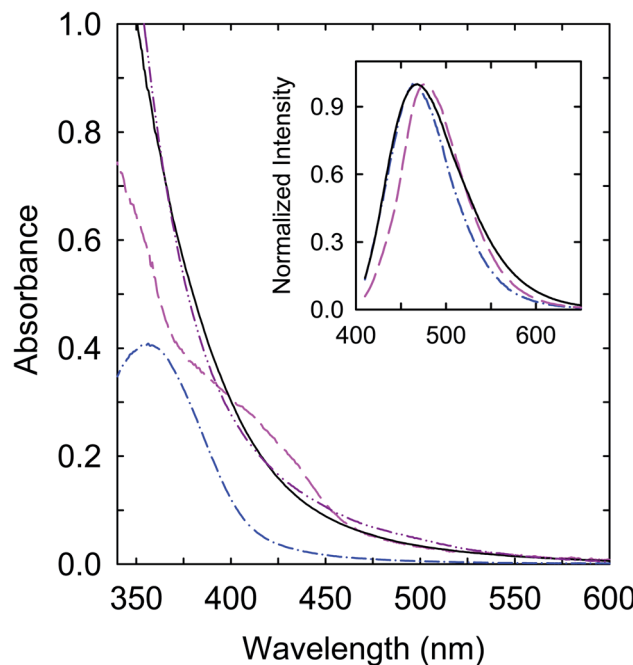


Fig. 2 Absorption and fluorescence (in the inset, 400 nm excitation) spectra of CS200 (dash-dot), CS330 (dash), and PEI-CDots (solid) in aqueous solutions. The absorption spectrum of the aqueous dispersed small carbon nanoparticles is also shown (dash-dot-dot) for comparison.

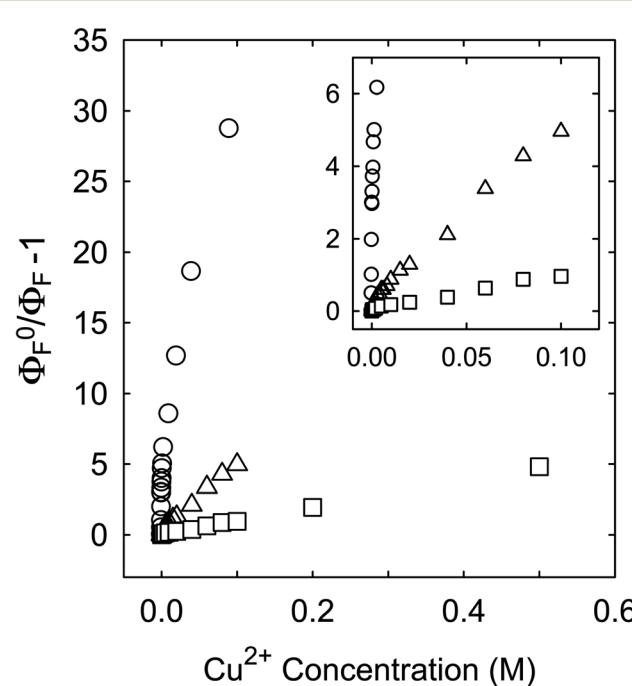


Fig. 3 Results on the quenching of fluorescence intensities of CS200 (circle), CS330 (triangle), and PEI-CDots (square) by Cu²⁺ in aqueous solutions. Inset: Enlarged for the low quencher concentration region.



the comparison between the three different dot samples (CS200, CS330, and PEI-CDots) in this work.

Fluorescence emission intensities (quantum yields) of all three samples were quenched by Cu^{2+} in aqueous solutions, but the dependencies of the quenching on Cu^{2+} concentrations were dramatically different between the three samples (Fig. 3). For CS200, the quenching was extremely efficient, with the quenching ratio Φ_F^0/Φ_F reaching ~ 30 at the very low Cu^{2+} concentration of only 0.09 M (Fig. 3). The quenching plot of $(\Phi_F^0/\Phi_F - 1)$ versus Cu^{2+} concentration is curved, from which the estimated slope as the quenching constant for the lower quencher concentration range (up to $2 \times 10^{-4} \text{ M}$) is about $10\,000 \text{ M}^{-1}$. A similar plot for the results of CS330 shows still highly efficient quenching, but relatively less so in comparison with that for CS200 (Fig. 3), with the estimated quenching constant of about 240 M^{-1} for the lower quencher concentration range (up to 10^{-3} M). The same quenching for PEI-CDots

was found to be much less efficient (Fig. 3), corresponding to the quenching constant of only about 10 M^{-1} .

Interestingly, despite the dramatically different efficiencies between the three dot samples in the quenching of their fluorescence emission intensities by Cu^{2+} , their fluorescence spectral profiles without and with the quenching are rather similar (Fig. 4), suggesting equally similar emissive excited states in the three different dot samples.

In addition to the steady-state measurements on the quenching of fluorescence emission intensities, fluorescence decays of the dot samples in aqueous solutions of varying Cu^{2+} concentrations were acquired and analyzed. In the decay measurements based on the time-correlated single photon counting technique, drops in the overall photon counts with the quenching by Cu^{2+} were very different between the three dot samples, generally in parallel with the trend found in the steady-state fluorescence quenching results discussed above. The observed fluorescence decays of all three dot samples without and with the quencher Cu^{2+} were non-exponential, as generally known for CDots.^{3,44} Nevertheless, the decay curves could be deconvoluted from the corresponding instrument response functions with the use of a bi-exponential function in the data fits, yielding two sets of pre-exponential factor and lifetime (A_1, τ_{F1} and A_2, τ_{F2}), which were used for the estimated average fluorescence lifetime $\langle \tau_F \rangle = (A_1 \tau_{F1}^2 + A_2 \tau_{F2}^2) / (A_1 \tau_{F1} + A_2 \tau_{F2})$.⁴³ The $\langle \tau_F \rangle$ values thus obtained for the three sample solutions excited at 400 nm are 12 ns for CS200, 13 ns for CS330, and 8.1 ns for PEI-CDots in the absence of any quenchers. With similarly determined average fluorescence lifetimes at different quencher Cu^{2+} concentrations, the quenching plots measuring the effects on fluorescence decays are compared in Fig. 5–7 with those on fluorescence intensities (taking the data from Fig. 3).

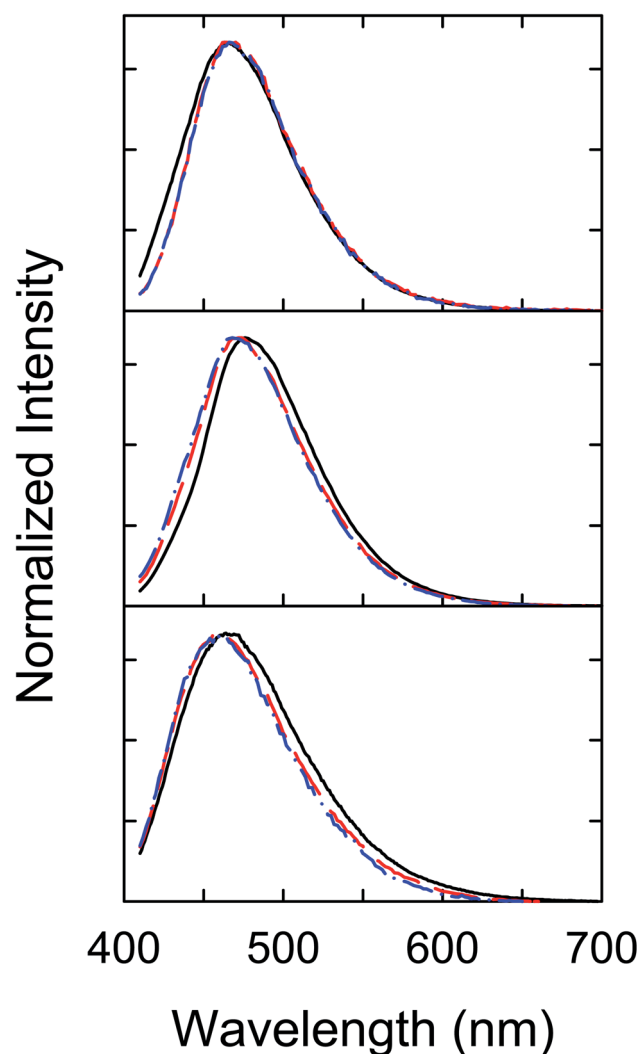


Fig. 4 Fluorescence spectral profiles (400 nm excitation) at different Cu^{2+} concentrations for CS200 (upper, solid: 0, dash: 0.04 M , and dash-dot: 0.09 M), CS330 (middle, solid: 0, dash: 0.04 M , and dash-dot: 0.1 M), and PEI-CDots (lower, solid: 0, dash: 0.2 M , and dash-dot: 0.5 M).

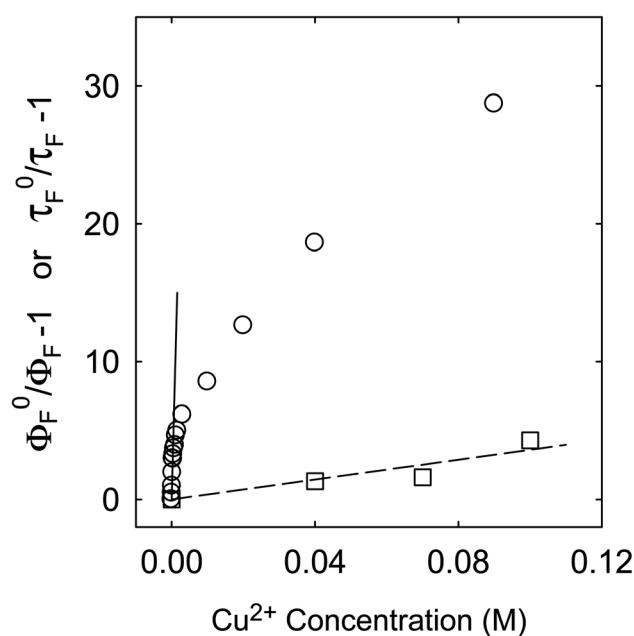


Fig. 5 For CS200, the quenching of fluorescence intensities (circle, solid line from fitting the data up to Cu^{2+} concentration of $2 \times 10^{-4} \text{ M}$) and lifetimes (square, dash line for the best fit).



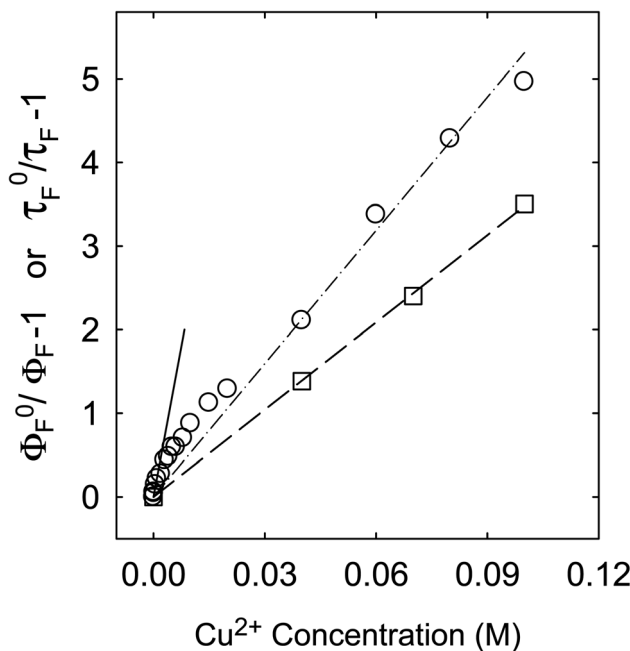


Fig. 6 For CS330, the quenching of fluorescence intensities (circle, solid line from fitting the data up to Cu^{2+} concentration of 10^{-3} M, and dash-dot line from a global fit of all data) and lifetimes (square, dash line for the best fit).

For the CS200 sample, the dramatic decoupling between quenching results for fluorescence intensities and lifetimes is rather obvious, with the former being considerably more efficient especially at low quencher concentrations (Fig. 5). By

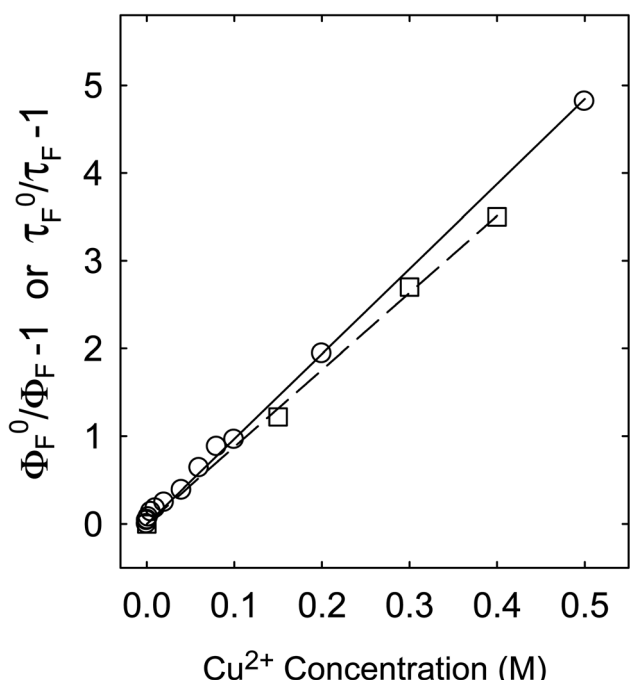


Fig. 7 For PEI-CDots, the quenching of fluorescence intensities (circle) and lifetimes (square), with solid and dash lines from best fits, respectively.

assuming that the slope of the quenching plot could be considered phenomenologically as Stern–Volmer constant ($K_{\text{SV}} = k_q \tau_F^0$), whose value of $10\,000\, \text{M}^{-1}$ over the low Cu^{2+} concentration range would require the quenching rate constant k_q to be more than $8 \times 10^{11}\, \text{M}^{-1}\, \text{s}^{-1}$ ($\tau_F^0 \sim 12\, \text{ns}$). It is simply impossible for k_q to actually reach such a level, because it is much beyond the limit of the diffusion rate constant in water (generally $10^{10}\, \text{M}^{-1}\, \text{s}^{-1}$ as the upper limit in organic solvents and lower in water). On the other hand, the quenching effects on fluorescence decays (and the estimated average fluorescence lifetimes) are large but still in the normal range, with the slope of the corresponding quenching plot $\sim 36\, \text{M}^{-1}$, within the general range of expected K_{SV} values for emissive excited states of nanosecond lifetimes. The corresponding k_q value of $3 \times 10^9\, \text{M}^{-1}\, \text{s}^{-1}$ is also within the constraint of diffusion control for the dynamic quenching process in an aqueous solution.

The similar decoupling between quenchings of fluorescence intensities and lifetimes was found for the CS330 sample, though the degree of decoupling was less dramatic and mostly at the low Cu^{2+} concentrations only (Fig. 6). For the quenching of intensities over the low Cu^{2+} concentrations up to 10^{-3} M, the slope of the quenching plot is about $240\, \text{M}^{-1}$, much smaller than that for the CS200 sample discussed above, but the corresponding k_q value of $1.85 \times 10^{10}\, \text{M}^{-1}\, \text{s}^{-1}$ still beyond the diffusion controlled limit. However, in a different data treatment by going beyond the low concentration region to take a global average with more weightings of quenchings at higher Cu^{2+} concentrations (Fig. 6), the resulting K_{SV} value of $\sim 53\, \text{M}^{-1}$ and the corresponding k_q value of $4 \times 10^9\, \text{M}^{-1}\, \text{s}^{-1}$ are not so far from those based on the quenching of fluorescence lifetimes (Figure 6), $35\, \text{M}^{-1}$ and $2.7 \times 10^9\, \text{M}^{-1}\, \text{s}^{-1}$, respectively, and the k_q values are both within the limit of diffusion control.

For the fluorescence quenching of PEI-CDots by Cu^{2+} in aqueous solutions, there is a much better agreement between those on intensities and lifetimes (Fig. 7), suggesting their same quenching mechanism and processes, with diminished local concentration effects. In fact, such an agreement is typical or “normal” for overwhelming majority of organic and other fluorophores (including conventional semiconductor quantum dots), namely that the dramatic or significant decoupling found for CS200 and CS330 samples is indicative of special fluorescence quenching behaviors, which may be associated with the different microscopic or nanoscale structures in those dot samples prepared by carbonization syntheses (Fig. 1).

In classical photophysics, the abnormally efficient fluorescence quenching at low quencher concentrations is generally attributed to local concentration effects, namely higher local quencher concentrations than the bulk due to more specific interactions of the quenchers with the emissive species being quenched, such as complex formation, association, or the like.⁴³ It results in near-neighbor quenching that is more “static” in nature, such that the quenching requires no or minimal diffusion of the quenchers, which is thus manifested by the extraordinarily large slope from the quenching plot. In fact, the slope thus obtained should not be equated with the K_{SV} in Stern–Volmer equation (contrary to what has been casually practiced in many literature reports) due to the specific underlying physical



meanings of the equation. Otherwise it would yield quenching rate constant k_q values larger than the limiting diffusion rate constant by orders of magnitude in many cases, which is simply impossible and wrong physically and photophysically. Instead, the observed extraordinarily efficient quenching of fluorescence intensities, especially at low quencher concentrations, for the CS200 and to a less extent CS330 samples in this work should be treated and understood by taking into consideration of local quencher (Cu^{2+}) concentration effects, with a modified Stern–Volmer equation: $\Phi_F^0/\Phi_F = 1 + K_{\text{SV}}[\text{Cu}^{2+}]_{\text{LOCAL}}$. For the quenching of fluorescence lifetimes, however, the fluorescence decay measurements on the nanosecond or sub-nanosecond time scale are incapable of capturing any contributions by near-neighbor static quenching (requiring no or very limited diffusions, often called “dark quenching” in photophysics textbooks), thus only the normal dynamic quenching correlated with the bulk quencher concentrations in terms of the (classical) Stern–Volmer equation.

For CS200, the much higher local quencher (Cu^{2+}) concentrations than the bulk are likely due to the expected porous characteristics of the dot-like species in the sample (Fig. 1), consistent with the sample preparation under rather mild processing conditions that are insufficient for substantial carbonization.^{3,19} The nanoscale carbon domains must be relatively small, probably serving the function of crosslinking the precursor organic species that survived the carbonization processing conditions. The microscopic or nanoscale structures in the sample may resemble sponges, which coupled with the presence of a substantial amount of amine moieties from the precursor PEI are amenable to adsorption-like accumulation of Cu^{2+} in the porous sample structures for the observed static quenching. The CS330 sample from more aggressive carbonization processing (higher temperature and longer time) should understandably contain more and relatively larger nanoscale carbon domains, though they are still mixed with a large amount of organic moieties (Fig. 1). The species in the sample may each be viewed as many small CDots-equivalent nanostructures that are linked/connected by organic moieties, significantly less porous for the sponging function discussed above for the CS200 sample, and consequently less local quencher concentration effects and the associated static quenching contributions. In fact, the nearly normal quenching behavior at high Cu^{2+} concentrations may be rationalized as being due to the saturation of the sponging function at the higher quencher concentrations. The structural characteristics of the CS200 and CS330 samples make them more appropriately described as “nano-carbon/organic hybrids” (Fig. 1), in which the individual species could be dot-like or in other shapes or configurations with adequate solubilities.

For PEI-CDots, clearly the nanostructures are dictated by the solid core carbon nanoparticles (Fig. 1), hardly sponge-like, so that the static quenching effects derived from higher than bulk local quencher concentrations are minimal at best, with the observed very similar quenching behaviors for both fluorescence intensities and lifetimes (Fig. 7).

The structural considerations on dot samples from carbonization processing of organic precursors (CS200 and CS330

specifically in this work) are consistent with the experimental results on quenchings of fluorescence intensities and lifetimes, though the proposed sponge-like porous characteristics in the solution phase are very difficult to be probed directly for verification. On the other hand, there are no justifications in principle or in terms of any direct experimental evidence on the presence of any thermodynamic and/or kinetic forces to drive the rather random and chaotic thermal carbonization processing to produce the specific and ordered nanostructure of classical CDots, which are both defined and experimentally verified as solid carbon nanoparticles surface-functionalized by the selected organic molecules (Fig. 1). Thus, to attribute the observed majorly different fluorescence quenching behaviors between the classical CDots and the carbonization-produced dot samples to their major differences in microscopic and nanoscale structures is justified.

Conclusions

Fluorescence quenching of both classical CDots and dot samples produced by the thermal carbonization of organic precursors can be used for the sensing of metal cations, Cu^{2+} specifically in this work. For the former, the quenching is within the framework of diffusion control. For the latter, however, the quenching of fluorescence intensities can be extraordinarily efficient due to substantial static quenching contributions associated with the higher than the bulk local quencher concentrations. The corresponding extraordinarily low detection limits, as claimed in many literature reports, may be beneficial in some applications, though in exchange for sacrifices in accuracy (due to the unpredictable nature of the local concentrations, for example) and reproducibility (due to variations in the dot samples associated with carbonization processing conditions that are intrinsically difficult to control and reproduce). A note here is that the accuracy and reproducibility are not those commonly considered in classical analytical chemistry. They refer to the potentially dramatic effects on the quenching results by small variations in the dot samples, which are unavoidable with the intrinsically chaotic carbonization processing despite all the efforts on keeping processing conditions the same in repeating syntheses. In any sensors, the obviously extreme sensitivity of the sensing (fluorescence quenching in this case) to changes in the sensor material is always a serious concern. More experimental and mechanistic correlations between the dot sample structures and fluorescence sensing outcomes are needed.

Experimental section

Materials

The carbon nanopowder sample (US1074) was acquired from US Research Nanomaterials, Inc. Citric acid was purchased from Alfa Aesar, oligomeric polyethylenimine (PEI, average molecular weight $M_w \sim 600$, branched) from Polyscience, Inc., and copper(II) nitrate from Fisher Scientific. Dialysis membrane tubing (molecular weight cut-off ~ 500 or 1000) was supplied by Spectrum



Laboratories. Water was deionized and purified by being passed through a Labconco WaterPros water purification system.

Measurement

UV/vis absorption spectra were recorded on Shimadzu UV2501 and UV-3600 spectrophotometers. Fluorescence spectra were acquired on a Jobin-Yvon emission spectrometer equipped with a 450 W xenon source, Gemini-180 excitation and Triax-550 emission monochromators, and a photon counting detector (Hamamatsu R928P PMT at 950 V). 9,10-Bis(phenylethynyl)-anthracene in cyclohexane was used as a standard in the determination of fluorescence quantum yields by the relative method. Fluorescence decays were measured by using the time-correlated single photon counting (TCSPC) technique on a Horiba Ultima Extreme spectrometer equipped with a SuperK Extreme supercontinuum laser source pulsed at 10 MHz, TDM-800 excitation and TDM-1200 emission monochromators, a R3809-50-MCP-PMT detector operated at 3 kV in a thermoelectrically cooled housing, and FluoroHub A++ timing electronics. The time resolution of the setup in terms of the instrument response function (IRF) is 100–250 ps, depending on excitation wavelengths. Experimental decay curves were deconvoluted by using the Dass6 decay analysis software. Fluorescence quenching experiments were performed with dot solutions of the constant optical density at the excitation wavelength less than 0.1, with the separately prepared Cu^{2+} solution added right before the fluorescence measurements.

Carbonization synthesis at 200 °C

Citric acid (1 g) and PEI (0.5 g) were mixed in water (10 mL), and the resulting mixture was loaded into a stainless steel tube reactor. With the reactor sealed, it was heated in a tube furnace at 200 °C for 3 h. Then, the reactor was cooled back to ambient, and the reaction mixture in the reactor was collected. The mixture was dialyzed (membrane pore size ~500) against fresh water, followed by concentration. A light brown aqueous solution was obtained as the sample from the carbonization synthesis at 200 °C (denoted as the sample CS200).

Carbonization synthesis at 330 °C

Citric acid (1 g) was dissolved in water (2 mL) with brief sonication, and the resulting solution was mixed well with PEI (0.5 g). Then, the mixture was loaded into a stainless steel tube reactor. With the reactor sealed, it was heated in a tube furnace at 330 °C for 6 h. Upon the cooling of the reactor back to ambient temperature, the reaction mixture in the reactor was collected by washing with water. The mixture was dialyzed (membrane pore size ~500) against fresh water. Upon concentration and then centrifugation, the colored supernatant was collected as an aqueous solution of the sample from the carbonization synthesis at 330 °C (denoted as the sample CS330).

PEI-CDots

The small carbon nanoparticles were harvested from the commercially acquired carbon nanopowder sample by

following the protocol reported previously.²⁴ Briefly, the carbon nanopowder sample (2 g) was refluxed in concentrated nitric acid (8 M, 200 mL) for 48 h. The reaction mixture was cooled back to the ambient temperature, followed by centrifuging at 1000g to discard the supernatant. The sediment was re-dispersed in deionized water, dialyzed in a membrane tubing (molecular weight cut-off ~500) against fresh water for 48 h, and then centrifuged at 1000g to retain the supernatant. Upon the removal of water *via* evaporation, the small carbon nanoparticles were obtained. These carbon nanoparticles were largely amorphous according to X-ray powder diffraction results.

The nanoparticles were used for the functionalization of PEI in the microwave-assisted thermal reaction. Briefly, the nanoparticle sample (100 mg) as an aqueous slurry was mixed with PEI (2 g) and ethanol (2 mL) in a scintillation vial with sonication in an ultrasonic cleaner (VWR 250D), followed by solvent evaporation for a solid mixture. Separately, a silicon carbide (150 g) bath in silica crucible casting dish (about 8 cm in diameter and 2.5 cm in height) was pre-heated in a conventional microwave oven at 500 W for 3 min. Several rounds of microwave heating were as follows: (1) the vial containing the solid mixture was immersed in the pre-heated silicon carbide bath for microwave irradiation at 1000 W for 3 min; (2) the sample vial was taken out of the bath and cooled to the ambient, and more PEI (1 g) and ethanol (2 mL) were added to the sample and mixed well, followed by the solvent evaporation and then microwave irradiation the same as in (1); (3) a repeat of (2) but with the microwave irradiation at 500 W for 8 min; and (4) a repeat of (3). The final reaction mixture was cooled to ambient and dispersed in deionized water with vigorous sonication. The resulting aqueous dispersion was centrifuged at 5000g to collect the supernatant, followed by dialysis (molecular weight cut-off ~1000) against fresh water for 6 h to obtain PEI-CDots in an aqueous solution.

Conflicts of interest

There are no conflicts to declare.

Acknowledgements

Financial support from Air Force Office of Scientific Research (AFOSR) through the program of Dr Kenneth Caster, Air Force Research Laboratory, and NSF (1855905, 1701399, and 1701424) is gratefully acknowledged. M. Z. was a participant of Palmetto Academy, a summer undergraduate research program of the South Carolina Space Grant Consortium.

References

- Y.-P. Sun, B. Zhou, Y. Lin, W. Wang, K. A. S. Fernando, P. Pathak, M. J. Meziani, B. A. Harruff, X. Wang, H. Wang, *et al.*, Quantum-Sized Carbon Dots for Bright and Colorful Photoluminescence, *J. Am. Chem. Soc.*, 2006, **128**, 7756–7757.
- Y.-P. Sun, Fluorescent Carbon Nanoparticles, *US Pat.*, 7829772, 2010.



3 Y.-P. Sun, *Carbon Dots – Exploring Carbon at Zero-Dimension*, Springer International Publishing, 2020.

4 P. G. Luo, S. Sahu, S.-T. Yang, S. K. Sonkar, J. Wang, H. Wang, G. E. LeCroy, L. Cao and Y.-P. Sun, Carbon “Quantum” Dots for Optical Bioimaging, *J. Mater. Chem. B*, 2013, **1**, 2116–2127.

5 C. Ding, A. Zhu and Y. Tian, Functional Surface Engineering of C-Dots for Fluorescent Biosensing and in Vivo Bioimaging, *Acc. Chem. Res.*, 2014, **47**, 20–30.

6 S. Y. Lim, W. Shen and Z. Gao, Carbon Quantum Dots and Their Applications, *Chem. Soc. Rev.*, 2015, **44**, 362–381.

7 K. A. S. Fernando, S. Sahu, Y. Liu, W. K. Lewis, E. A. Gulians, A. Jafariyan, P. Wang, C. E. Bunker and Y.-P. Sun, Carbon Quantum Dots and Applications in Photocatalytic Energy Conversion, *ACS Appl. Mater. Interfaces*, 2015, **7**, 8363–8376.

8 X. Gao, C. Du, Z. Zhuang and W. Chen, Carbon Quantum Dot-based Nanoprobe for Metal Ion Detection, *J. Mater. Chem. C*, 2016, **4**, 6927–6945.

9 G. A. M. Hutton, B. C. M. Martindale and E. Reisner, Carbon Dots as Photosensitisers for Solar-Driven Catalysis, *Chem. Soc. Rev.*, 2017, **46**, 6111–6123.

10 M. Hassan, V. G. Gomes, A. Dehghani and S. M. Ardekani, Engineering Carbon Quantum Dots for Photomediated Theranostics, *Nano Res.*, 2018, **11**, 1–41.

11 J. Du, N. Xu, J. Fan, W. Sun and X. Peng, Carbon Dots for In Vivo Bioimaging and Theranostics, *Small*, 2019, **15**, 1805087.

12 M. J. Molaei, Carbon Quantum Dots and Their Biomedical and Therapeutic Applications: A Review, *RSC Adv.*, 2019, **9**, 6460–6481.

13 D. Xu, Q. Lin and H.-T. Chang, Recent Advances and Sensing Applications of Carbon Dots, *Small Methods*, 2019, 1900387.

14 P. Devi, P. Rajput, A. Thakur, K.-H. Kim and P. Kumar, Recent Advances in Carbon Quantum Dot-Based Sensing of Heavy Metals in Water, *Trends Anal. Chem.*, 2019, **114**, 171–195.

15 X. Dong, W. Liang, M. J. Meziani, Y.-P. Sun and L. Yang, Carbon Dots as Potent Antimicrobial Agents, *Theranostics*, 2020, **10**, 671–686.

16 Y. Xu, H. Yu, L. Chudal, N. K. Pandey, E. H. Amador, B. Bui, L. Wang, X. Ma, S. Deng, X. Zhu, S. Wang and W. Chen, Striking Luminescence Phenomena of Carbon Dots and Their Applications as a Double Ratiometric Fluorescence Probes for H₂S Detection, *Materials Today Physics*, 2021, **17**, 100328.

17 X. Tang, H. Yu, B. Bui, L. Wang, C. Xing, S. Wang, M. Chen, Z. Hua and W. Chen, Nitrogen-Doped Fluorescence Carbon Dots as Multi-Mechanism Detection for Iodide and Curcumin in Biological and Food Samples, *Bioact. Mater.*, 2021, **6**, 1541–1554.

18 L. Cao, K. A. S. Fernando, W. Liang, A. Seilkop, L. M. Veca, Y.-P. Sun and C. E. Bunker, Carbon Dots for Energy Conversion Applications, *J. Appl. Phys.*, 2019, **125**, 220903.

19 W. Liang, C. E. Bunker and Y.-P. Sun, Carbon Dots: Zero-Dimensional Carbon Allotrope with Unique Photoinduced Redox Characteristics, *ACS Omega*, 2020, **5**, 965–971.

20 H. P. Liu, T. Ye and C. D. Mao, Fluorescent Carbon Nanoparticles Derived from Candle Soot, *Angew. Chem., Int. Ed.*, 2007, **46**, 6473–6475.

21 S. C. Ray, A. Saha, N. R. Jana and R. Sarkar, Fluorescent Carbon Nanoparticles: Synthesis, Characterization, and Bioimaging Application, *J. Phys. Chem. C*, 2009, **113**, 18546–18551.

22 L. Cao, P. Anilkumar, X. Wang, J.-H. Liu, S. Sahu, M. J. Meziani, E. Myers and Y.-P. Sun, Reverse Stern-Volmer Behavior for Luminescence Quenching in Carbon Nanoparticles, *Can. J. Chem.*, 2011, **89**, 104–109.

23 Y. Liu, Y. Liu, H. Qian, P. Wang, G. E. LeCroy, C. E. Bunker, K. A. S. Fernando, L. Yang, M. Reibold and Y.-P. Sun, Carbon-TiO₂ Hybrid Dots in Different Configurations – Optical Properties, Redox Characteristics, and Mechanistic Implication, *New J. Chem.*, 2018, **42**, 10798–10806.

24 F. Yang, G. E. LeCroy, P. Wang, W. Liang, J. Chen, K. A. S. Fernando, C. E. Bunker, H. Qian and Y.-P. Sun, Functionalization of Carbon Nanoparticles and Defunctionalization - Towards Structural and Mechanistic Elucidation of Carbon “Quantum” Dots, *J. Phys. Chem. C*, 2016, **120**, 25604–25611.

25 D. G. Yoo, Y. Park, B. Y. Cheon and M.-H. Park, Carbon Dots as an Effective Fluorescent Sensing Platform for Metal Ion Detection, *Nanoscale Res. Lett.*, 2019, **14**, 272.

26 Y. Q. Dong, R. X. Wang, G. L. Li, C. Q. Chen, Y. W. Chi and G. N. Chen, Polyamine-Functionalized Carbon Quantum Dots as Fluorescent Probes for Selective and Sensitive Detection of Copper Ions, *Anal. Chem.*, 2012, **84**, 6220–6224.

27 A. Salinas-Castillo, M. Ariza-Avidad, C. Pritz, M. Camprubí-Robles, B. Fernandez, M. J. Ruedas-Rama, A. Megia-Fernandez, A. Lapresta-Fernandez, F. Santoyo-Gonzalez, A. Schrott-Fischer and L. F. Capitan-Vallvey, Carbon Dots for Copper Detection with Down and Upconversion Fluorescent Properties as Excitation Sources, *Chem. Commun.*, 2013, **49**, 1103–1105.

28 J. Chen, Y. Li, K. Lv, W. B. Zhong, H. Wang, Z. Wu, P. G. Yi and J. H. Jiang, Cyclam-Functionalized Carbon Dots Sensor for Sensitive and Selective Detection of Copper (II) Ion and Sulfide Anion in Aqueous Media and its Imaging in Live Cells, *Sens. Actuators, B*, 2016, **224**, 298–306.

29 J. M. Liu, L. P. Lin, X. X. Wang, S. Q. Lin, W. L. Cai, L. H. Zhang and Z. Y. Zheng, Highly Selective and Sensitive Detection of Cu²⁺ with Lysine Enhancing Bovine Serum Albumin Modified-Carbon Dots Fluorescent Probe, *Analyst*, 2012, **137**, 2637–2642.

30 P. Das, S. Ganguly, M. Bose, S. Mondal, A. K. Das, S. Banerjee and N. C. Das, A Simplistic Approach to Green Future with Eco-friendly Luminescent Carbon Dots and Their Application to Fluorescent Nano-Sensor “Turn-Off” Probe for Selective Sensing of Copper Ions, *Materials Science and Engineering C*, 2017, **75**, 1456–1464.

31 R. Yang, X. Guo, L. Jia and Y. Zhang, A Fluorescent “On-Off-On” Assay for Selective Recognition of Cu (II) and Glutathione Based on Modified Carbon Nanodots, and Its Application to Cellular Imaging, *Microchim. Acta*, 2017, **184**, 1143–1150.

32 H. M. R. Gonçalves, A. J. Duarte and J. C. G. Esteves da Silva, Optical Fiber Sensor for Hg(II) Based on Carbon Dots, *Biosens. Bioelectron.*, 2010, **26**, 1302–1306.



33 Y. Xiong, J. Schneider, E. V. Ushakova and A. L. Rogach, Influence of Molecular Fluorophores on the Research Field of Chemically Synthesized Carbon Dots, *Nano Today*, 2018, **23**, 124–139.

34 S. Khan, A. Sharma, S. Ghoshal, S. Jain, M. K. Hazra and C. K. Nandi, Small Molecular Organic Nanocrystals Resemble Carbon Nanodots in Terms of Their Properties, *Chem. Sci.*, 2018, **9**, 175–180.

35 V. Hinterberger, C. Damm, P. Haines, D. M. Guldin and W. Peukert, Purification and Structural Elucidation of Carbon Dots by Column Chromatography, *Nanoscale*, 2019, **11**, 8464–8474.

36 W. Liang, L. Ge, X. Hou, X. Ren, L. Yang, C. E. Bunker, C. M. Overton, P. Wang and Y.-P. Sun, Evaluation of Commercial “Carbon Quantum Dots” Sample on Origins of Red Absorption and Emission Features, *C*, 2019, **5**, 70.

37 Y. Dong, R. Wang, W. Tian, Y. Chi and G. Chen, “Turn-on” Fluorescent Detection of Cyanide Based on Polyamine-Functionalized Carbon Quantum Dots, *RSC Adv.*, 2014, **4**, 3685–3689.

38 X. Hou, Y. Hu, P. Wang, L. Yang, M. M. Al Awak, Y. Tang, F. K. Twara, H. Qian and Y.-P. Sun, Modified Facile Synthesis for Quantitatively Fluorescent Carbon Dots, *Carbon*, 2017, **122**, 389–394.

39 X. Dong, L. Ge, D. I. Abu Rabe, O. O. Mohammed, P. Wang, Y. Tang, S. Kathariou, L. Yang and Y.-P. Sun, Photoexcited State Properties and Antibacterial Activities of Carbon Dots Relevant to Mechanistic Features and Implications, *Carbon*, 2020, **170**, 137–145.

40 X. Ren, W. Liang, P. Wang, C. E. Bunker, M. Coleman, L. R. Teisl, L. Cao and Y.-P. Sun, A New Approach in Functionalization of Carbon Nanoparticles for Optoelectronically Relevant Carbon Dots and Beyond, *Carbon*, 2019, **141**, 553–560.

41 X. Wang, L. Cao, F. Lu, M. J. Meziani, H. Li, G. Qi, B. Zhou, B. A. Harruff, F. Kermarrec and Y.-P. Sun, Photoinduced Electron Transfers with Carbon Dots, *Chem. Commun.*, 2009, 3774–3776.

42 J. B. Birks, *Photophysics of Aromatic Molecules*, John Wiley & Sons, 1970.

43 J. R. Lakowicz, *Principles of Fluorescence Spectroscopy*, 2nd edn, Kluwer Academic/Plenum Publishers, New York, 1999.

44 G. E. LeCroy, F. Messina, A. Sciotino, C. E. Bunker, P. Wang, K. A. S. Fernando and Y.-P. Sun, Characteristic Excitation Wavelength Dependence of Fluorescence Emissions in Carbon “Quantum” Dots, *J. Phys. Chem. C*, 2017, **121**, 28180–28186.

